Earth's radiation belts ions: patterns of the spatial-energy structure and its solar-cyclic variations

Alexander S. Kovtyukh
Skobeltsyn Institute of Nuclear Physics, Moscow State University, Moscow, 119234, Russia;
kovtyukhas@mail.ru

Abstract Spatial-energy distributions of the stationary fluxes of protons, helium and ions of carbon-nitrogen-oxygen (CNO) group, with energy from $E \sim 100$ keV to 200 MeV, in the Earth's radiation belts (ERB), at $L \sim 1$–8, are considered here using data from satellites in the period 1961–2017. ~~It is find~~ It has been found that the results of these measurements line up in the space $\{E, L\}$ following ~~by~~ some regular patterns. The ion ERB shows a single intensity peak that moves toward Earth with increasing energy and decreasing ion mass. Solar-cyclic (11-year) variations in the distributions of protons, helium and CNO group ions fluxes in the ERB are studied. It has been observed that in the inner regions of the ERB, fluxes decrease with increasing solar activity and that the solar-cyclic variations of fluxes of $Z \geq 2$ ions are much greater than for protons; moreover, it seems that they increase with increasing atomic number Z. ~~Finally, the possible physical mechanisms leading to formation of this spatial-energy structure and to the solar-cyclic variations of the ERB ion fluxes are discussed~~. It is suggested that heavier ion intensities peak further from the Earth and vary more over the solar cycle because they have more strong ionization losses. These results indicate also that with variations in the level of solar activity the coefficient D_{LL} of the radial diffusion of the ERB ions change much less than the ionization loss rates of ions with $Z \geq 2$.

Keywords. Magnetospheric physics (energetic particles, trapped). Radiation belts.

1 Introduction

The ERB consist mainly of charged particles with energy from $E \sim 100$ keV to several hundreds of megaelectronvolt (MeV). These particles are trapped by the geomagnetic field at altitudes from ~ 200 kilometers to ~ 50–70 thousands kilometers. The ERB ~~is consisted~~ consists mainly of electrons and protons, but there are also helium nuclei and other $Z > 2$ ions (like oxygen etc), where Z is the charge of the atomic nucleus with respect to the charge of the proton. During geomagnetic disturbances, ion fluxes, and their distributions are changed. These fluxes depend also on the phase of the solar cycle, conditions in the interplanetary space, and other factors.

Particles with different energy E and pitch angles α (α is the angle between the local vector of the magnetic field and the vector of a particle velocity), which are injected into some point of the geomagnetic trap, drift conserving the adiabatic invariants (μ, K, Φ) ~~and populate a narrow layer surrounding~~ around the Earth (Alfvén and Fälthammar, 1963; Northrop, 1963). ~~This layer is called the drift shells.~~ Therefore, experimental data on the ERB are often represented in coordinates $\{L, B\}$, where L is the drift shell parameter and B is the local induction of the magnetic field (McIlwain, 1961). For the dipole magnetic field, L is a distance, in the equatorial plane, from the given magnetic field line to the center of the dipole itself (in Earth's radii R_E).

The stationary fluxes J of the ERB particles with given energy and pitch angle α decrease usually when the point of observation is shifted from the equatorial plane to higher latitudes along a certain magnetic field line (if we exclude the peripheral regions of the geomagnetic trap, where the drift shells of the captured particles are split and branched). This dependence is described by the functions $J(B/B_0)$, were B and B_0 are values of the magnetic field at the point of observation and in the equatorial plane on the same magnetic field line, respectively.

Outer and inner regions of the ERB are maintained in dynamic equilibrium with the environment by different mechanisms (see review Kovtyukh, 2018).

The outer belt ($L > 3.5$) is formed mainly by the mechanisms of radial diffusion of ions towards the Earth under the action of fluctuations of both electric and magnetic fields resonating with their drift periods (see, e.g., Schulz and Lanzerotti 1974; Kovtyukh, 2016b). This transport is accompanied by the betatron acceleration and by the ionization losses of the ions as a result of their interactions with the plasmasphere and with residual atmosphere.

The inner belt ($L < 2.5$) of protons with $E > 10$ MeV is formed mainly as a result of decay of neutrons knocked from the nuclei of the atmospheric atoms by the Galactic Cosmic Rays (GCR)~~.~~ ~~For~~ ; for protons with $E < 10$ MeV this, mechanism (CRAND) is supplemented by the radial diffusion of particles from the outer to the inner belt (see, e.g., Selesnick et al., 2013, 2014). The inner belt of ions with $Z > 4$ is formed mainly from the ions of the Anomalous component of Cosmic Rays (see, e.g., Mazur et al., 2000).

In the intermediate region ($2.5 < L < 3.5$), the mechanism of a ion capture from Solar Cosmic Rays takes place during strong magnetic storms (see, e.g., Selesnick et al., 2014).

Thus, the main mechanisms of formation of the ERB, together with the sources of injection and losses of ions, are known. However, for a comprehensive verification of the physical models and to identify the mathematical models and their parameters, the formulation of complete and reliable empirical representations of the ERB for each of the ion components, is necessary; it is also necessary for ensuring the safety of space flights.

These models can be created only using experimental data, obtained over many years and decades; such models (see, e.g., Ginet et al., 2013) were already created for protons (AP8/AP9) and they are widely used in space research. On the contrary, measurements of $Z \geq 2$ ion fluxes suffer from technical problems due to small statistics and high background of protons and electrons. For this reasons, empirical and semi-empirical models for $Z \geq 2$ ions, are applicable only to very limited regions of the space $\{E, L\}$.

One of the main problems of this work is to consider the possibility to create sufficiently complete and reliable empirical models of the ERB for these ions based on currently available experimental data.

In the following sections, the spatial-energy structure of the ERB in the $\{E, L\}$ space for protons, helium and CNO group ions are considered (Sect. 2) together with possible physical mechanisms of formation of these structures and their solar-cyclic variations (Sect. 3). Finally, the main conclusions of this work are given (Sect. 4).

2 Spatial-energy distributions of the ion fluxes near the equatorial plane

There can be ions trapped in drift shells only with energies less than some maximum values, determined by the Alfvén's criterion: $\rho_i(L, E, M_i, Q_i) << R_c(L)$, where ρ_i is the gyroradius of ions, and R_c is the radius of curvature of the magnetic field near the equatorial plane (M_i and Q_i are mass and charge of ions with respect to the corresponding values for protons). According to this criterion and to the theory of stochastic motion of particles, the geomagnetic trap in the dipolar region can capture and durably hold only ions with E (MeV) $< 2000\times(Q_i^2/M_i)\ L^{-4}$ (Ilyin et al., 1984). The green line in Figs 1-6 represents this very boundary.

When comparing the data of various experiments in the ERB, the question arises about the compatibility of these results with each other and the reasons for their discrepancies. A significant number of these discrepancies can be connected to the differences in their trajectories; in the construction of the instruments and their angular characteristics; in the energy ranges and sets of energy channels. For the stationary ERB, these discrepancies can also be associated with differences in the general state of the Sun, heliosphere and magnetosphere of the Earth during various periods of data-taking. These factors influence the fluxes of ions with $Z \geq 2$ in the ERB more significantly with respect to proton fluxes (see, e.g., Kovtyukh, 2018).

In this section, experimental data of various satellites, which were obtained for quiet periods (Kp < 2) and near the equatorial plane of the ERB for ions with equatorial pitch angles $\alpha_0 \approx 90^o$ have been used. In the regions of E and L shells, where these data were obtained, the ion fluxes ~~do~~ are not distorted by the background of other particles.

In many important experiments, the instruments were not able to separate fluxes of ions by their charge. Moreover, for the ions of the CNO group, the separation by mass are not usually performed. For heavier species, for example for Fe ions, we have very small data-sets. Therefore, this work presents data on helium ions (without any charge separating) and CNO ions (without any mass or charge separation).

To solve the aforementioned problems, it is important to choose the form of representation (space of variables), in which the results of every experiment can be compared to the others. In our case, the space $\{E. L\}$ has been used; this choice is very efficient to better organize fragmentary experimental data obtained in different ranges of E and L.

Figures 1–6 show the spatial-energy distributions of the fluxes of protons, helium ions, and ions of the CNO group near the equatorial plane. Odd figures refer to periods near the minima, and even figures refer to periods near the solar activity maxima. The values E and L in these figures are presented in logarithmic scales. Statistical and methodical errors of the experimentalal points on these figures do not exceed of the size of these points. The markers are connected by lines of equal intensity of ion fluxes (iso-lines); the decimal logarithms of the fluxes J, in unit of $(\text{cm}^2\ \text{s ster MeV/n})^{-1}$, are shown near each iso-lines.

Such representations of the experimental data are not only visual, but also very convenient and rather universal. Obviously, Figs. 1–6 actually show both radial profiles of the fluxes of ions for a given energy and ion energy spectra for a given L shell.

The points in Figs. 1–6 have been obtained from the radial profiles of fluxes $J(L)$ for the average energies of the ions in the channels of the instruments. Unlike electron fluxes or ion fluxes

measured during geo-active conditions, the ion fluxes considered here (i.e. during quiet periods), have only one maximum in the functions $J(L)$. As a result, for each ~~experiment~~ energy channel of the respective mission, 1 or 2 points were obtained (on the outer and inner edges of these profiles) with certain values of E and L for a given level of ion fluxes. Sometimes, especially for fluxes, only one point was obtained: in these cases, the radial profile of the ion fluxes was cutoff at small values of L due to a significant background of contaminating particles and no interpolation/extrapolation has been performed whatsoever.

Each iso-line, shown in these figures, has been evaluated separately from the corresponding set of experimental points (icons); then it was transferred (along with the icons) to the corresponding figure; thus, in more abundantly populated sectors of the plots (i.e. for protons with $E > 1$ MeV at $L > 2$) such iso-lines are mixing in Figs. 1–2. In case of a large distance between neighboring points, the corresponding segments of the iso-lines are shown as dashed arcs.

The radial profiles of the differential fluxes $J(L)$ of particles with different energy tend to intersect with each other in those regions where the energy spectra present some local maximum or minimum. On the contrary, the iso-lines cannot intersect with each other: because this would mean that, at the same point in the space $\{E, L\}$, the ion fluxes differ very significantly (by an order of magnitude) for quiet periods. Such uncertainty does not have a physical sense and a special analysis is needed to identify other possible sources of errors.

Representing plots in a different space of variables would lead to more significant methodological errors and uncertainties, because of the natural differences in the instrumentation of the experiments taken into account; thus, a series of approximations or interpolation/extrapolation techniques would become inevitable.

2.1 Spatial-energy structure of the proton fluxes

There is a large number of experimental data concerning ERB protons; the most important of them are presented in Figs. 1 and 2. These figures serve as a comparison with similar distributions of $Z \geq 2$ ions (Figs. 3–6).

Figure 1 sums up results from the satellites Relay-1 (Freden et al., 1965); Ohzora or EXIS C: Exospheric Satellite C, Akebono or EXOS-D: Exospheric Satellite D and ETS-VI: Engineering Test Satellite (Goka et al., 1999). These results have been collected during minimum periods of various solar cycles, i.e. between 19^{th} / 20^{th} (1963), 21^{th} / 22^{th} (1984–1985), and 22^{th} / 23^{th} (1994–1996) of the solar activity cycles.

Figure 2 sums up results from the satellites 1968-81A (Stevens et al., 1970), Injun-5 or Explorer-40 (Krimigis, 1970; Venkatesan and Krimigis, 1971; Pizzella and Randall, 1971), 1969-025C or OV1-19: Orbiting Vehicle 1-19 (Croley et al., 1976), Azur or GRS A: German Research Satellite A (Hovestadt et al., 1972; Westphalen and Spjeldvik, 1982), Molniya-1 (Panasyuk and Sosnovets, 1973), GEOS-2: Geodetic Earth Orbiting Satellite 2 (Wilken et al., 1986), CRRES: The Combined Release and Radiation Effects Satellite (Albert et al., 1998; Vacaresse et al., 1999), GEO-3: Geostationary Orbit 3 (Selesnick et al., 2010) and Van Allen Probes (Selesnick et al., 2014, 2018). These results were obtained during maximum periods of 20^{th} (1968–1971), 22^{th} (1990–1991), 23^{th} (2000), and 24^{th} (2012–2017) solar cycles.

The data of the satellites Explorer-45 (Fritz and Spjeldvik, 1979, 1981) and ISEE-1: International Sun-Earth Explorer 1 or Explorer-56 (Williams, 1981; Williams and Frank, 1984) are given in both Figs. 1 and 2 because solar-cyclic variations of the ERB proton fluxes are negligible at $L > 2.5$ (see, e.g., Vacaresse et al., 1999).

From a comparison of Figs. 1 and 2, one can see that at $L < 2.5$ (especially at $L < 1.4$) the proton fluxes during solar minima (Fig. 1) are higher than during maxima (Fig. 2). In addition, in the former the inner edge of the proton belt is less steep and it can reach smaller L shells (for $E > 1$ MeV). The distributions of protons in the space $\{\mu, L\}$ (see, e.g., Kovtyukh,(2016a,b) , which ~~I~~ have been constructed from Figs. 1 and 2 confirm these conclusions.

In Figs. 1 and 2, the iso-lines of proton fluxes are almost parallel to each other on $L > 3$ at sufficiently high energies. Since these iso-lines have separated from each other by approximately equal intervals on a logarithmic scale of the energy, this region in the space $\{E. L\}$ corresponds to power-law spectra of the ERB protons: for power-law spectra, $J \propto E^{-\gamma}$, where the index $\gamma = -\Delta(\log J)/\Delta(\log E)$. In these figures, this region is located between the green and red lines.

The red line corresponds to the lower boundary (E_b) of the power-law tail of the proton spectra. For this line, $E_b \sim 36 \times L^{-3}$ MeV. Some changes in the slope of these iso-lines at $L > 6$ can be connected to a discrepancy between the real configuration of the magnetic field lines and the dipolar configuration (used here for L shells calculation and for the red line).

For the dipole magnetic field region, the points on the red line correspond to particles with a specific value of the 1st adiabatic invariant of motion (μ_b). For Figs. 1 and 2, the average value μ_b is ~ 1.16 keV nT^{-1}. Segments of an iso-lines, that are parallel to the red line, also correspond to certain values of the invariant μ. In this region of the space $\{E. L\}$ the ionization and other losses of the ERB protons during radial drift can be neglected, and changes of fluxes with changing L are practically reduced to adiabatic transformations in a magnetic field.

It results from these figures that at L = 3–6, the value $\gamma = 4.8 \pm 0.5$. At $L > 6$ the distances between these iso-lines increase with L, and the value γ is decreased from ~ 4.7–5.0 at $L = 6$ to ~ 4.1–4.5 at $L = 8$. This is due to the deviation of the magnetic field from the dipole configuration as well as to the increasing variability of this field with increasing L.

According to the data of satellites considered in (Kovtyukh, 2001), invariant parameters μ_b and γ were found only at $L > 3$. In this work, a wider range of L and E is considered, and for protons with $E > 10$ MeV these parameters can be traced to $L \sim 2$. At $L = 2$, $\gamma = 4.4 \pm 0.6$ (Fig. 1) and $\gamma = 4.7 \pm 1.3$ (Fig. 2). This is due to the fact that the energy range is significantly extended toward higher values (up to 200 MeV), but here the ionization losses for protons rapidly decrease (see, e.g., Schulz and Lanzerotti, 1974; Kovtyukh, 2016a).

2.2 Spatial-energy structure of the helium ion fluxes

In Figs. 3 and 4 helium ion fluxes, averaged for quiet periods (Kp < 2), are presented.

Figure 3 sums up results from the satellites Molnija-2 (Panasyuk et al., 1977), Prognoz-5 (Lutsenko and Nikolaeva, 1978), ISEE-1: The International Sun-Earth Explorer 1 (Hovestadt et al., 1981); Akebono or EXOS-D: Exospheric Satellite D and ETS-VI: Engineering Test Satellite (Goka et al., 1999). These results have been collected during minimum periods of various solar cycles, i.e. between 20th / 21th (1975–1977), 21th / 22th (1984–1985), and 22th / 23th (1994–1996) of the solar activity cycles.

Figure 4 sums up results from the satellites OV1-19: Orbiting Vehicle 1-19 (Blake et al., 1973; Fennell and Blake, 1976), Explorer-45 (Fritz and Spjeldvik, 1978, 1979; Spjeldvik and Fritz, 1981), SCATHA: Spacecraft Charging At High Altitudes (Blake and Fennell, 1981; Chenette et al., 1984). These results were obtained during maximum periods of 20th (1968–1971) and 21th (1979) solar cycles.

From a comparison of Figs. 1–2 with Figs. 3–4, one can see that at $L > 2$ for helium ions the solar-cyclic (11-year) variations are greater than for protons. For example, at $L \sim 2$–3 from maximum to minimum of solar activity fluxes of protons with $E > 1$ MeV practically do not changed, and the fluxes of helium ions with $E > 1$ MeV/n are increased by one order of magnitude.

Figures 3 and 4 show the same patterns as for protons, but the distribution of helium ion fluxes is slightly shifted towards higher values of L shell (with respect to protons). Unlike protons, there are significant "white spots" in these figures because there are no experimental data for helium ions in these regions.

The red line on these figures corresponds to the lower boundary of the power-law tail of the helium ions spectra. For this line, $E_b/M_i \sim 43.4 \times L^{-3}$ MeV/n (Fig. 3) and $E_b/M_i \sim 21.7 \times L^{-3}$ MeV/n

(Fig. 4). If one takes into account that at $L < 6$ for helium ions with $E > 0.2$ MeV/n the average charge $Q_i = +2$ (see, e.g, Spjeldvik, 1979), then for the considered boundary we get: $\mu_b \sim 1.4 \times Q_i$ keV/n×nT^{-1} at the maximum of solar activity and $\mu_b \sim 1.4 \times M_i$ keV/n×nT^{-1} at the minimum of solar activity (for the dipole magnetic field region). The iso-lines of helium ion fluxes in Figs. 3 and 4, which pass above the red line at $L > 2.5$, correspond to an average value of $\gamma \sim 5.5$ (there is a large uncertainty due to the small covered energy range).

For helium spectra, as for protons ones, the values of the parameters of the power-law tail are in ~~good~~ agreement with what has been found in (Kovtyukh, 2001).

At the same time, one can see that the iso-lines of the fluxes of helium ions in the region above the red line (i.e. in the region of power-law spectra) substantially deviate from the slope of the red line. At $L > 3$ the fluxes of helium ions with given energy are increase with decreasing L slower than it is for protons ~~expected from adiabatic transformation~~. This means that the ionization losses of the ERB helium ions significantly exceed these losses for protons, in agreement to well-known calculations (see, e.g., Schulz and Lanzerotti, 1974). For example, Coulomb loss rate increases with increasing Z of the ions as Z^2.

2.3 Spatial-energy structure of the CNO group ions fluxes

In Figs. 5 and 6 CNO group ions fluxes, averaged for quiet periods (Kp < 2), are presented.

Figure 5 sums up results from the satellites ATS-6: Applications Technology Satellite 6 (Spjeldvik and Fritz, 1978; Fritz and Spjeldvik, 1981) and ISEE-1: The International Sun-Earth Explorer 1 (Hovestadt et al., 1978). These results have been collected during minimum period between 20th / 21th of the solar activity cycles (1974–1975, 1977).

Figure 6 sums up results from the satellite Explorer-45 (Spjeldvik and Fritz, 1978; Fritz and Spjeldvik, 1981). These results were obtained during maximum period of activity in 20th solar cycle (1971–1972).

On Figs. 5–6 the spatial-energy patterns of the ion fluxes of the CNO group are even more shifted towards higher values of L shell and its configuration differ significantly from Figs. 1–4.

From a comparison of Figs. 1–2 with Figs. 5–6 one can see that, for ions of CNO group, the solar-cyclic (11-year) variations are greater than for protons. For example, at $L \sim 3$–5 from maximum to minimum of solar activity fluxes of protons with $E > 1$ MeV practically do not changed, but the fluxes of the CNO group increase by one order of magnitude or more. From a comparison of Figs. 3–4 with Figs. 5–6 it is seen also that the fluxes of CNO group change several times more than the fluxes of helium ions do.

This means that, for ions of the CNO group, the ionization losses at $L = 3$–5 are much larger than for ions with $Z \leq 2$ and these losses have a significant effect even on the power-law segment of the spectra of the CNO ions (in the part which is seen on Figs. 5–6). Therefore, the lower boundary of the power-law tail of these ions spectra have not been obtained by the experiments collected in Figs. 5 and 6. The red line on these figures corresponds to adiabatic laws (see Kovtyukh, 2001); this line let us estimate the deviations from these laws. As can be seen from Fig. 5–6, ionization losses for ions of the CNO group are especially large at the peak of solar activity (Fig. 6): during these times, the slope of iso-lines on $L > 3$ is significantly less than the slope of the red line.

At the same time, at $L > 4$ in Fig. 5 and at $L > 3$ in Fig. 6, the iso-lines of fluxes pass almost parallel to each other and at approximately equal distances from each other; the average value of γ corresponding to them is ~ 6 (there is a large uncertainty due to the small covered energy range). Thus, for sufficiently large values of E and L, the CNO group ions spectra in the ERB have a power-law form, but these spectra are softer in comparison with the spectra of protons.

The red line corresponds here to the dependences $E_b/M_i \approx 43.4 \times L^{-3}$ MeV/n (on Fig. 5) and $E_b/M_i \sim 12.4 \times L^{-3}$ MeV/n (on Fig. 6), which are taken from (Kovtyukh, 2001) where this boundary was

more clearly defined also for the ions of the CNO group. If one takes into account that at $L \sim 3$–5 for the CNO group ions with $E > 0.1$ MeV/n the average charge $Q_i = +4$ (see, e.g., Spjeldvik and Fritz, 1978), then for this boundary one can get: $\mu_b \sim 1.4 \times Q_i$ keV/n×nT^{-1} at the maximum of solar activity and $\mu_b \sim 1.4 \times M_i$ keV/n×nT^{-1} at the minimum of solar activity (for the dipole magnetic field region).

3 Discussion

Let us consider the conclusions following the results obtained here for solar-cyclic variations in the fluxes of ERB ions. Solar-cyclic (11-year) variations of proton fluxes with $E > 1$ MeV in the inner region of the ERB have been studied in many works (see, e.g., Pizzella et al., 1962; Hess, 1962; Blanchard and Hess, 1964; Filz, 1967; Nakano and Heckman, 1968; Vernov, 1969; Dragt, 1971; Huston et al., 1996; Vacaresse et al., 1999; Kuznetsov et al., 2010; Qin et al., 2014). These variations reach one order of magnitude at $L = 1.14$ and are reduced rapidly with increasing L (see, e.g., Vacaresse et al., 1999). However, solar-cyclic variations of fluxes of ions with $Z \geq 2$ have not been considered in these works.

In these works, such variations of the proton fluxes of the inner belt are connected to the solar-cyclic variations of the energy loss rates of protons in this region. ~~However, solar-cyclic variations of fluxes of ions with $Z \geq 2$ have not been considered in these works.~~ For protons with E> 10 MeV of the inner ERB, the effect of attenuation of GCR proton fluxes in the Earth's orbit with increasing solar activity acts in the same direction (see, e.g., Usoskin et al., 2005; Selesnick et al., 2007). We must also take into account a secular variations of the geomagnetic dipole moment (see, e.g., Selesnick et al., 2007).

Consider in more detail the solar-cyclic variations of the ERB ions fluxes in connect to variations of the energy loss rates of these ions. In quiet periods, only the mechanism of ionization loss is significant for the ERB protons trapped in small L shells (see, e.g., Schulz and Lanzerotti, 1974). Energy loss rates and lifetimes of the ERB protons are determined, in this mechanism, by the density of atmospheric atoms and ionospheric plasma (N) in a geomagnetic trap. This density depends on the intensity of the ultraviolet radiation of the Sun. With decreasing solar activity (with a transition from maximum to minimum of the solar cycle), the densities of atmospheric atoms and ionospheric plasma in a geomagnetic trap are decreased~~. If the proton supply rates to the inner belt, under the action of the CRAND mechanism, remain unchanged or the effect of these changes is weaker than the effect connected with changes of loss rates of the protons,~~ and the stationary proton fluxes will increase with decreasing solar activity.

The lifetimes of protons increase with L; this leads to a decrease in the amplitude of the solar-cyclic variations of proton fluxes. A proton lifetime on a given L shell depends on its energy and is less than 11 years ($\sim 3.5 \times 10^8$ s) at $L < L_c(E)$. For example, for protons with $E > 6$ MeV the value L_c is ~ 2.5 and corresponds to protons with $\mu > 3$ keV nT^{-1} (see, e.g., Kovtyukh, 2016b, Fig. 3). Figs. 1 and 2 show that for protons the solar-cyclic variations of fluxes are small and localized at $L < 2.5$ (mainly at $L < 1.4$).

In contrast to protons, Figs. 3–6 show significant solar-cyclic variations of fluxes of helium ions and CNO group ions at $L \sim 2$–5. There is low density of atmospheric atoms and ionospheric plasma in that region (compared to $L < 2$), but the density is changes consistently with solar cycle. ~~These variations can be explained by the same mechanism that has been suggested for protons at $L < 2.5$.~~

For ions with $Z \geq 2$ in the ERB, ionization losses are more significant than for protons and this can be connected to the absence of ions with $Z \geq 2$ at $L < 2$ (or very low values of these fluxes) during quiet geomagnetic conditions. Such short lifetimes are manifested also in the slope of the experimental curves in Fig. 4 and 6 (this was noted in sections 2.2 and 2.3, respectively).

Consequently, for ions with $Z \geq 2$, the regions in which variations can manifested, should be located on higher L shells (at the same energies as for protons).

The lifetimes of ions in the energy ranges considered here are $\tau \propto M_i^{-1/2} Q_i^{-2} N^{-1} E^{3/2}$ (Schulz and Lanzerotti, 1974). In a first approximation, for $N \propto L^{-4}$, we obtain the value $L_{ci} \sim M_i^{1/8} Q_i^{1/2} L_c$, where L_c corresponds to the L shell of protons of the same energy of the other ions under study. For helium ions ($M_i = 4$, $Q_i = 2$) with $E \sim 6$ MeV, we obtain outer boundary $L_{ci} \sim 4.2$. For ions of CNO group ($M_i = 14$, $Q_i = 4$) with $E \sim 6$ MeV we obtain outer boundary $L_{ci} \sim 6.9$. These are very rough estimations, but they are in agreement with the results presented in Figs. 3–6.

These estimates are based on the following assumption: during variations in solar activity, the rates of ion supply on $L < L_{ci}$ remains unchanged (or these changes are weaker than the effect of changes of the rate of ion losses). This assumption is real for protons with $E > 10$–20 MeV at $L < 2.2$: ; in fact, these protons form mainly under the action of the CRAND mechanism. However, at $L > 2.2$ the The stationary ion fluxes of the ERB at $L > 2.5$ form mainly under the action of radial diffusion (see, e.g., Schulz and Lanzerotti, 1974; Kovtyukh, 2016b, 2018). Therefore, the solar-cyclic variations of $Z \geq 2$ ion fluxes can be motivated only under the assumption that the effect related with an increase in the ionization losses of such ions significantly exceeds the effect connected with the possible enhance of radial diffusion of ions during the rising phase of solar activity. For example, when compare the empirical model of the inner belt ($L < 2.4$) of protons with $E \sim 19$–200 MeV, constructed on the data of Van Allen Probes satellites, with the mathematical model of radial diffusion of protons in this region, it was assumed that on the phase of growth of solar activity from 2013 to 2015, D_{LL} increases by ~ 2 times (Selesnick and Albert, 2019).

In the experimental results presented here for the ERB ions, the region of the power-law tail of the ion spectra is distinguished. For many experiments, especially for heavy ions, the values of the parameter of a power-law tail spectra are determined much more accurately by the dependences $J(L)$ of the ion fluxes (in logarithmic scale) for different pairs of energy channels (see Kovtyukh, 2001). For example, the range of L, in which these dependences for two energy channels are parallel to each other is connected to the power-law tail of the spectra. Instead, on smaller values of L, these fluxes begin to converge and the radial dependences of these fluxes intersect with each other, which is related to the maximum in the spectra.

The main source of ions in the outer regions of the ERB is the solar wind, and usually the high-energy part of these spectra have an exponential shape (see, e.g., Ipavich et al., 1981a, 1981b). Immediately before being captured into the magnetosphere, these ions pass through a highly turbulized regions, but the high-energy part of their spectra usually retains an exponential shape. Therefore, the question arises: what physical mechanism converts the form of ion spectra from exponential to power-law?

Evidently, the power-law tail of the ERB ions spectra must be generated in the outer regions of the magnetosphere. The most likely region for this to happen is the plasma sheet (PS) of the magnetospheric tail, which is adjacent to the geomagnetic trap. The high-energy part of the ion spectra in the PS, at $R \sim 20$–40 R_E, has a power-law shape and the exponents of these spectra are close to the corresponding parameters of the spectra of ions in the ERB. On the data of the satellites IMP-7 and IMP-8 (Sarris et al., 1981; Lui et al., 1981) and also satellite ISEE-1 (Christon et al., 1991), the shape of the ion spectra of the PS usually do not change during substorms; they produce only parallel shifts of the spectra along logarithmic axes E and J. These results point out that the time scales of formation processes of these ion spectra in the PS exceed the times of substorms.

Parameters of the power-law tail of the ion spectra of the outer belt (γ and μ_b) reflect, apparently, the most fundamental features of the mechanisms of acceleration of ions in the tail of the magnetosphere. One can try to connect the values of these parameters with the most general representations of the mechanisms of ion acceleration in the PS of the magnetospheric tail.

Most likely, this part of the ion energy spectra is formed in the PS by stochastic mechanisms of ion acceleration; this hypothesis is supported by many experimental results. The statistical aspect of these mechanisms reveals itself, in particular, in the fact that the ratios of fluxes (and partial densities) of ions with different Z can differ, even greatly, at low and high energies. During their wander in the phase space, ions gradually loose information about their origin and, therefore, the high-energy tails of their spectra contain ambiguous information on the partial densities of different components of ions in the source (see, e.g., Kovtyukh, 2001).

The high-energy part of the ion spectra of the PS can be generated by the mechanisms of acceleration of particles on magnetic irregularities moving with respect to each other (Fermi mechanism). The fractal structures of the PS are revealed on scales from ~ 0.4 to ~ 8 thousands kilometers, for example, in the data of the satellite Geotail (Milovanov et al., 1996). ~~If the mass of the ions are small compared to the mass of the magnetic irregularities in the PS, the average values of the index γ of the power-law tail should not depend on mass and charge of such nuclei.~~

Under equilibrium conditions, this parameter is determined by the average part of energetic ions in the total energy density of particles and magnetic irregularities ($\overline{\beta}$). From the theory which was developed by Ginzburg and Syrovatskii (1964), it follows: $\gamma - 1 \approx (1 - \overline{\beta})^{-1}$. With increasing $\overline{\beta}$ in the interval $0 < \overline{\beta} < 1$, the value γ ~~is~~ increases monotonically and $\gamma \to \infty$ for $\overline{\beta} \to 1$. For real average values $\overline{\beta}$ in the central PS $\overline{\beta}$ = 0.6–0.7 (see, e.g., Baumjohann, 1993, Fig. 1), we get γ = 3.5–4.3 ~~~ 3.5–7.0 (γ ~ 4.3 at $\overline{\beta}$ ~ 0.7)~~.

Spectra with power-law tail and quasi-exponential segment at lower energies can be generated when the value $\Delta B / \overline{B}$ for magnetic irregularities is proportional to their size δr and their spectral density decreases rapidly with increasing δr for $\delta r < r_s$ (r_s is a thickness of the central PS), but for $\delta r > r_s$ it remains almost unchanged. Apparently, the spectra of magnetic irregularities in the PS ~~with thickness r_s~~ have just such form (see, e.g., Milovanov et al., 1996). Then, the lower boundary μ_b of the power-law tail corresponds to the condition $r_s/\rho_i \sim 10$, where ρ_i is the gyroradius of ions (see, e.g., Alfvén and Fälthammar, 1963), i.e. $\mu_b \sim 0.02(Q_i^2/M_i)B_s r_s^2$ keV nT^{-1}, where B_s is the average magnetic field induction in the PS (in nT) and r_s is normalized to the Earth's radius. Using $B_s \sim 30$ nT and $r_s \sim 1.3$ R_E (see, e.g., Baumjohann, 1993) it can be obtained: $\mu_b \sim 1.0\ (Q_i^2/M_i)$ keV nT^{-1}. This value is similar to the lower boundary of the power law spectrum which we find for the ERB protons, suggesting that not only the slope of the spectrum but also its validity range can be explained with scattering at magnetic irregularities.

The energy spectra of ions in the radiation belts of such planets as Jupiter and Saturn have the form analogous to that of ion spectra in the ERB (see, e.g., Krimigis et al., 1981; Cheng et al., 1985; Kollmann et al., 2011). As that in the ERB, these spectra have a long power-law tail, which is formed, apparently, by mechanisms of stochastic acceleration of ions as a result of their interactions with the current layer of the magnetospheric tail.

4 Conclusions

In this work, the experimental results for the stationary fluxes of the main ion components of the ERB (protons, helium ions and ions of the CNO group) in the near equatorial~~ly~~ plane, have been analyzed. It is has been found that in the outer belt these fluxes line up in the certain regular patterns in the space $\{E, L\}$. The degree of ~~such~~ similarity increases with increasing E and L and it is linked to the nature of the main sources and on the universality mechanisms of transfer, acceleration and losses of ERB ions in the outer belt (radial diffusion which conserves μ and K of ions, betatron acceleration and ionization losses).

Moreover, solar-cyclic (11-year) variations of the spatial-energy distributions of the ERB ion fluxes have been investigated. It has been noted that the ERB ions fluxes are weaker with increasing solar activity and this effect increases with increasing atomic number Z. This kind of

dependence of the amplitude of flux changes on Z is typical, also, for faster variations in the fluxes of the ERB ions, during geomagnetic storms and other disturbances of the Earth's magnetosphere, as has been underlined in the review Kovtyukh (2018).

The figures presented here make it possible to determine in which regions of the space $\{E, L\}$ near the equatorial plane the ionization losses of ions during their radial diffusion can be neglected and where this cannot. These results indicate also that with variations in the level of solar activity the coefficient D_{LL} of the radial diffusion of the ERB ions change much less than the ionization losses rates of ions with $Z \geq 2$.

In addition, the figures given here reveal the localization of "white spots", especially extensive for ions with $Z \geq 2$ and $E > 1$ MeV/n at $L < 3$. As Z and energy become larger and L becomes smaller, the uncertainties in the values of the ERB fluxes become larger. These gaps must be filled by the results of future experiments on satellites; for now, the extensive gaps in $Z \geq 2$ ion data do not allow to create sufficiently complete and reliable empirical models of the ERB for these ions.

Acknowledgements. The author would like to thank the reviewers, Anonymous Referee #1 and Peter Kollmann (Applied Physics Laboratory, Johns Hopkins University), for very important and fruitful comments and proposals to the paper.

Financial support. This work was supported by Russian Foundation for Basic Research RFFI grant No. 17-29-01022.

References

Alfvén, H., and Fälthammar, C.-G.: Cosmical Electrodynamics, Fundamental Principles, Clarendon Press, Oxford, 1963.

Albert, J. M., Ginet, G. P., and Gussenhoven, M. S.: CRRES observations of radiation belt protons, 1, Data overview and steady state radial diffusion, J. Geophys. Res., **103**(A5), 9261–9273. https://doi.org/10.1029/97JA02869, 1998.

Baumjohann, W.: The near-Earth plasma sheet: An AMPTE/IRM perspective, Space Sci. Rev., **64**(1–2), 141–163, https://doi.org/10.1007/BF00819660, 1993.

Blake, J. B., and Fennell, J. F.: Heavy ion measurements in the synchronous altitude region, Planet. Space Sci., **29**(11), 1205–1213, https://doi.org/10.1016/0032.0633(81)90125-2, 1981.

Blake, J. B., Fennell, J. F., Schulz, M., and Paulikas, G. A.: Geomagnetically trapped alpha particles, 2, The inner zone, J. Geophys. Res., **78**(25), 5498–5506, https://doi.org/10.1029/JA078i025p05498, 1973.

Blanchard, R. C., and Hess, W. N.: Solar cycle changes in inner-zone protons, J. Geophys. Res., **69**(19), 3927–3938, https://doi.org/10.1029/JZ069i019p03927, 1964.

Chenette, D. L., Blake, J. B., and Fennell, J. F.: The charge state composition of 0.4–MeV helium ions in the Earth's outer radiation belts during quiet times, J. Geophys. Res., **89**(A9), 7551–7555, https://doi.org/10.1029/JA089iA09p07551, 1984.

Cheng, A. F., Krimigis, S. M., and Armstrong, T. P.: Near equality of ion phase space densities at Earth, Jupiter, and Saturn, J. Geophys. Res., **90**(A9), 526–530, http://doi.org/10.1029/JA090iA01p00526, 1985.

Christon, S. P., Williams, D. J., Mitchell, D. G., Huang, C. Y., and Frank, L. A.: Spectral characteristics of plasma sheet ion and electron populations during disturbed geomagnetic conditions, J. Geophys. Res., **96**(A1), 1–22, https://doi.org/10.1029/90JA01633, 1991.

Croley, D. R., Jr., Schulz, M., and Blake, J. B.: Radial diffusion of inner-zone protons: Observations and variational analysis, J. Geophys. Res., **81**(4), 585–594, https://doi.org/10.1029/JA081i004p00585, 1976.

Dragt, A. J.: Solar cycle modulation of the radiation belt proton flux, J. Geophys. Res., **76**(10), 2313–2344, https://doi.org/10.1029/JA076i010p02313, 1971.

Fennell, J. F., and Blake, J. B.: Geomagnetically trapped α-particles, Magnetospheric Particles and Fields, edited by: McCormac, B. M., D. Reidel, Dordrecht, Holland, 149–156, 1976.
Filz, R. C.: Comparison of the low-altitude inner-zone 55–MeV trapped proton fluxes measured in 1965 and 1961–1962, J. Geophys. Res., **72**(3), 959–963, https://doi.org/10.1029/JZ072i003p00959, 1967.
Freden, S. C., Blake, J. B., and Paulikas, G. A.: Spatial variation of the inner zone trapped proton spectrum, J. Geophys. Res., **70**(13), 3113–3116, https://doi.org/10.1029/JZ070i013p03113, 1965.
Fritz, T. A., and Spjeldvik, W. N.: Observations of energetic radiation belt helium ions at the geomagnetic equator during quiet conditions, J. Geophys. Res., **83**(A6), 2579–2583, https://doi.org/10.1029/JA083iA06p02579, 1978.
Fritz, T. A., and Spjeldvik, W. N.: Simultaneous quiet time observations of energetic radiation belt protons and helium ions: The equatorial α/p ratio near 1 MeV, J. Geophys. Res., **84**(A6), 2608–2618, https://doi.org/10.1029/JA084iA06p02608, 1979.
Fritz, T. A., and Spjeldvik, W. N.: Steady-state observations of geomagnetically trapped energetic heavy ions and their implications for theory, Planet. Space Sci., **29**(11), 1169–1193, https://doi.org/10.1016/0032-0633(81)90123-9, 1981.
Ginzburg, V. L., and Syrovatskii, S. I.: The Origin of Cosmic Rays, Pergamon Press, Oxford, 1964.
Ginet, G. P., O'Brien, T. P., Huston, S. L., Johnston, W. R., Guild, T. B., Friedel, R., Lindstrom, C. D., Roth, C. J., Whelan, P., Quinn, R. A., Madden, D., Morley, S., and Su, Yi-J.: AE9, AP9 and SPM: New models for specifying the trapped energetic particle and space plasma environment, Space Sci. Rev., **179**(1–4), 579–615, https://doi.org/10.1007/s11214-013-9964-y, 2013.
Goka, T., Matsumoto, H., and Takagi, S.: Empirical model based on the measurements of the Japanese spacecrafts, Radiation Measurements, **30**(5), 617–624, https://doi.org/10.1016/S1350-4487(99)00237-1, 1999.
Hess, W. N.: Discussion of paper by Pizzella, McIlwain, and Van Allen, 'Time variations of intensity in the Earth's inner radiation zone, October 1959 through December 1960', J. Geophys. Res., **67**(12), 4886–4887, https://doi.org/10.1029/JZ0670i012p04886, 1962.
Hovestadt, D., Häusler, B., and Scholer, M.: Observation of energetic particles at very low altitudes near the geomagnetic equator, Phys. Rev. Lett., **28**(20), 1340–1343, https://doi.org/10.1103/PhysRevLett.28.1340, 1972.
Hovestadt, D., Gloeckler, G., Fan, C. Y., Fisk, L. A., Ipavich, F.M., Klecker, B., O'Gallagher, J. J., and Scholer, M.: Evidence for solar wind origin of energetic heavy ions in the Earth's radiation belt, Geophys. Res. Lett., **5**(12), 1055–1057, https://doi.org/10.1029/GL005i012p01055, 1978.
Hovestadt, D., Klecker, B., Mitchell, E., Fennell, J. F., Gloeckler, G., and Fan, C. Y.: Spatial distribution of $Z \geq 2$ ions in the outer radiation belt during quiet conditions, Adv. Space Res., **1**(1), 305–308, https://doi.org/10.1016/0273-1177(81)90125-3, 1981.
Huston, S., Kuck, G., and Pfitzer, K.: Low-altitude trapped radiation model using TIROS/NOAA data, Radiation Belts: Models and Standards, edited by: Lemaire, J. F., Heynderickx, D., and Baker, D. N., AGU, Washington, D. C., 119–122, https://doi.org/10.1029/GM097/p0119, 1996.
Ilyin, B. D., Kuznetsov, S. N., Panasyuk, M. I., and Sosnovets, E.N.: Non-adiabatic effects and boundary of the trapped protons in the Earth's radiation belts, Bulletin of the Russian Academy of Sciences: Physics, **48**(11), 2200–2203, 1984.
Ipavich, F. M., Galvin, A. B., Gloeckler, G., Scholer, M., and Hovestadt D.: A statistical survey of ions observed upstream of the Earth's bow shock: Energy spectra, composition, and spatial variation, J. Geophys. Res., **86**(A6), 4337–4342, https://doi.org/10.1029/JA086iA06p4337, 1981a.

Ipavich, F. M., Scholer, M., and Gloeckler, G.: Temporal development of composition, spectra, and anisotropies during upstream particle events, J. Geophys. Res., **86**(A13), 11153–11160, https://doi.org/10.1029/JA086iA13p11153, 1981b.
Kollmann, P., Roussos, E., Paranicas, C., Krupp, N., Jackman, C. M., Kirsch, E., and Glassmeier, K.-H.: Energetic particle phase space densities at Saturn: Cassini observations and interpretations, J. Geophys. Res. Space Phys., **116**(A5), A05222, https://doi.org/10.1029/2010JA016221, 2011.
Kovtyukh, A. S.: Geocorona of hot plasma, Cosmic Res., **39**(6), 527–558, https://doi.org/10.1023/A:1013074126604, 2001.
Kovtyukh, A. S.: Radial dependence of ionization losses of protons of the Earth's radiation belts, Ann. Geophys., **34**(1), 17–28, https://doi.org/10.5194/angeo-34-17-2016, 2016a.
Kovtyukh, A. S.: Deduction of the rates of radial diffusion of protons from the structure of the Earth's radiation belts, Ann. Geophys., 34(11), 1085–1098. https://doi.org/10.5194/angeo-34-1085-2016, 2016b.
Kovtyukh, A. S.: Ion Composition of the Earth's Radiation Belts in the Range from 100 keV to 100 MeV/nucleon: Fifty Years of Research, Space Sci. Rev., **214**(8), 124:1–124:30, https:/doi.org/10.1007/s11214-018-0560-z, 2018.
Krimigis, S. M.: Alpha particles trapped in the Earth's magnetic field, Particles and Fields in the Magnetosphere, edited by: McCormac, B. M., D. Reidel, Dordrecht, Holland, 364–379, 1970.
Krimigis, S. M., Carbary, J. F., Keath, E. P., Bostrom, C. O., Axford, W. I., Gloeckler, G., Lanzerotti, L. J., and Armstrong, T. P.: Characteristics of hot plasma in the Jovian magnetosphere: Results from the Voyager spacecraft, J. Geophys. Res., **86**(A10), 8227–8257. http://doi.org/10.1029/JA086iA10p08227, 1981.
Kuznetsov, N. V., Nikolaeva, N. I., and Panasyuk, M. I.: Variation of the trapped proton flux in the inner radiation belt of the Earth as a function of solar activity, Cosmic Res., **48**(1), 80–85, https://doi.org/10.1134/S0010952510010065, 2010.
Lui, A. T. Y., and Krimigis, S. M.: Several features of the earthward and tailward streaming of energetic protons (0.29–0.5 MeV) in the Earth's plasma sheet, J. Geophys. Res., **86**(A13), 11173–11188, https://doi.org/10.1029/JA086iA13p11173, 1981.
Lutsenko, V. N., and Nikolaeva, N. S.: Relative content and the range of alpha particles in the inner radiation belt of the Earth by measurements on satellite Prognoz-5, Cosmic Res., **16**(3), 459–462, 1978.
Mazur, J. E., Mason, G. M., Blake, J. B., Klecker, B., Leske, R. A., Looper, M. D., and Mewaldt, R. A.: Anomalous cosmic ray argon and other rare elements at 1–4 MeV/nucleon trapped within the Earth's magnetosphere, J. Geophys. Res., **105**(A9), 21015–21023, https://doi.org/10.1029/1999JA000272, 2000.
McIlwain, C. E.: Coordinate for mapping the distribution of magnetically trapped particles, J. Geophys. Res., **66**(11), 3681–3691, https://doi.org/10.1029/JZ066i011p03681, 1961.
Milovanov, A. V., Zelenyi, L. M., and Zimbardo, G.: Fractal structures and power low spectra in the distant Earth's magnetotail, J. Geophys. Res. Space Phys., **101**(A9), 19903–19910, https://doi.org/10.1029/96JA01562, 1996.
Nakano, G., and Heckman, H.: Evidence for solar-cycle changes in the inner-belt protons, Phys. Rev. Lett., **20**(15), 806–809, https://doi.org/10.1103/PhysRevLett.20.806, 1968.
Northrop, T. G.: The Adiabatic Motion of Charged Particles, Wiley-Interscience, NY, USA, 1963.
Panasyuk, M. I., and Sosnovets, E. N.: Differential energy spectrum of low-energy protons in the inner region of the radiation belt, Cosmic Res., **11**(3), 436–440, 1973.
Panasyuk, M. I., Reizman, S. Ya., Sosnovets, E. N., and Filatov, V. N.: Experimental results of protons and α-particles measurements with energy more 1 MeV/nucleon in the radiation belts, Cosmic Res., **15**(6), 887–894, 1977.

Pizzella, G., McIlwain, C. E., and Van Allen, J. A.: Time variations of intensity in the Earth's inner radiation zone, October 1959 through December 1960, J. Geophys. Res., **67**(4), 1235–1253, https://doi.org/10.1029/JZ0670i004p01235, 1962.

Pizzella, G., and Randall, B. A.: Differential energy spectrum of geomagnetically trapped protons with the Injun 5 satellite, J. Geophys. Res., **76**(10), 2306–2312, https://doi.org/10.1029/JA076i010p02306, 1971.

Qin, M., Zhang, X., Ni, B., Song, H., Zou, H., and Sun, Y.: Solar cycle variations of trapped proton flux in the inner radiation belt, J. Geophys. Res. Space Phys., **119**(12), 9658–9669, https://doi.org/10.1002/2014JA020300, 2014.

Sarris, E. T., Krimigis, S. M., Lui, A. T. Y., Ackerson, K. L., Frank, L. A., and Williams, D. J.: Relationship between energetic particles and plasmas in the distant plasma sheet, Geophys. Res. Lett., **8**(4), 349–352, https://doi.org/10.1029/GL008i004p0349, 1981.

Schulz, M., and Lanzerotti, L. J.: Particle Diffusion in the Radiation Belts, Springer, NY, USA, 1974.

Selesnick, R. S., Looper, M. D., and Mewaldt, R. A.: A theoretical model of the inner proton radiation belt, Space Weather, **5**(4), S04003, https://doi.org/10.1029/2006SW000275, 2007.

Selesnick, R. S., Hudson, M. K., and Kress, B. T.: Injection and loss of inner radiation belt protons during solar proton events and magnetic storms, J. Geophys. Res. Space Phys., **115**(A8), A08211, https://doi.org/10.1029/2010JA015247, 2010.

Selesnick, R. S., Hudson, M. K., and Kress B. T.: Direct observation of the CRAND proton radiation belt source, J. Geophys. Res. Space Phys., **118**(12), 7532–7537, https://doi.org/10.1002/2013JA019338, 2013.

Selesnick, R. S., Baker, D. N., Jaynes, A. N., Li, X., Kanekal, S. G., Hudson, M. K., and Kress, B. T.: Observations of the inner radiation belt: CRAND and trapped solar protons, J. Geophys. Res. Space Phys., **119**(8), 6541–6552, https://doi.org/10.1002/2014JA020188, 2014.

Selesnick, R. S., Baker, D. N., Kanekal, S. G., Hoxie, V. C., and Li, X.: Modeling the proton radiation belt with Van Allen Probes Relativistic Electron-Proton Telescope data, J. Geophys. Res. Space Phys., **123**(1), 685–697, https://doi.org/10.1002/2017JA024661, 2018.

Selesnick, R. S., and Albert, J. M.: Variability of the proton radiation belt, J. Geophys. Res. Space Phys., **124**(7), 5516–5527, https://doi.org/10.1029/2019JA026754, 2019.

Spjeldvik, W. N.: Expected charge states of energetic ions in the magnetosphere, Space Sci. Rev., **23**(3), 499–538, https://doi.org/10.1007/BF00172252, 1979.

Spjeldvik, W. N., and Fritz, T. A.: Quiet time observations of equatorially trapped megaelectronvolt radiation belt ions with nuclear charge $Z \geq 4$, J. Geophys. Res., **83**(A9), 4401–4405, https://doi.org/10.1029/JA083iA09p04401, 1978.

Spjeldvik, W. N., and Fritz, T. A.: Observations of energetic helium ions in the Earth's radiation belts during a sequence of geomagnetic storms, J. Geophys. Res., **86**(A4), 2317–2328, https://doi.org/10.1029/JA086iA04p02317, 1981.

Stevens, J. R., Martina, E. F., and White, R. S.: Proton energy distributions from 0.060 to 3.3 MeV at 6.6 Earth radii, J. Geophys. Res., **75**(28), 5373–5385, https://doi.org/10.1029/JA075i028p05373, 1970.

Usoskin, I. G., Alanko-Huotari, K., Kovaltsov, G, A., and Mursula, K.: Heliospheric modulation of cosmic rays: Monthly reconstruction for 1951–2004, J. Geophys. Res., **110**(A12), A12108, https://doi.org/10.1029/2005JA011250, 2005.

Vacaresse, A., Boscher, D., Bourdarie, S., Blanc, M., and Sauvaud, J. A.: Modeling the high-energy proton belt, J. Geophys. Res. Space Phys., **104**(A12), 28601–28613, https://doi.org/10.1029/1999JA900411, 1999.

Venkatesan, D., and Krimigis, S. M.: Observations of low-energy (0.3– to 1.8–MeV) differential spectrums of trapped protons, J. Geophys. Res., **76**(31), 7618–7631, https://doi.org/10.1029/JA076i031p07618, 1971.

Vernov, S. N.: The Earth's radiation belts. In G. Bozóki, E. Gombosi, A. Sebestyén, A. Somogyi

(Eds.), Proc. 11th ICRC, Budapest, 85–162, 1969.
Westphalen, H., and Spjeldvik, W.N.: On the energy dependence of the radial diffusion coefficient and spectra of inner radiation belt particles: Analytic solution and comparison with numerical results, J. Geophys. Res., **87**(A10), 8321–8326, https://doi.org/10.1029/2000JA087iA10p08321, 1982.
Wilken, B., Baker, D. N., Higbie, P. R., Fritz, T. A., Olson, W. P., and Pfitzer, K. A.: Magnetospheric configuration and energetic particle effects associated with a SSC: A case study of the CDAW 6 event on March 22, 1979, J. Geophys. Res., **91**(A2), 1459–1473, https://doi.org/10.1029/JA091iA02p01459, 1986.
Williams, D. J.: Phase space variations of near equatorially mirroring ring current ions, J. Geophys. Res., **86**(A1), 189–194, https://doi.org/10.1029/JA086iA01p00189, 1981.
Williams, D. J., and Frank, L. A.: Intense low-energy ion populations at low equatorial altitude, J. Geophys. Res., **89**(A6), 3903–3911, https://doi.org/10.1029/JA089iA06p03903, 1984.

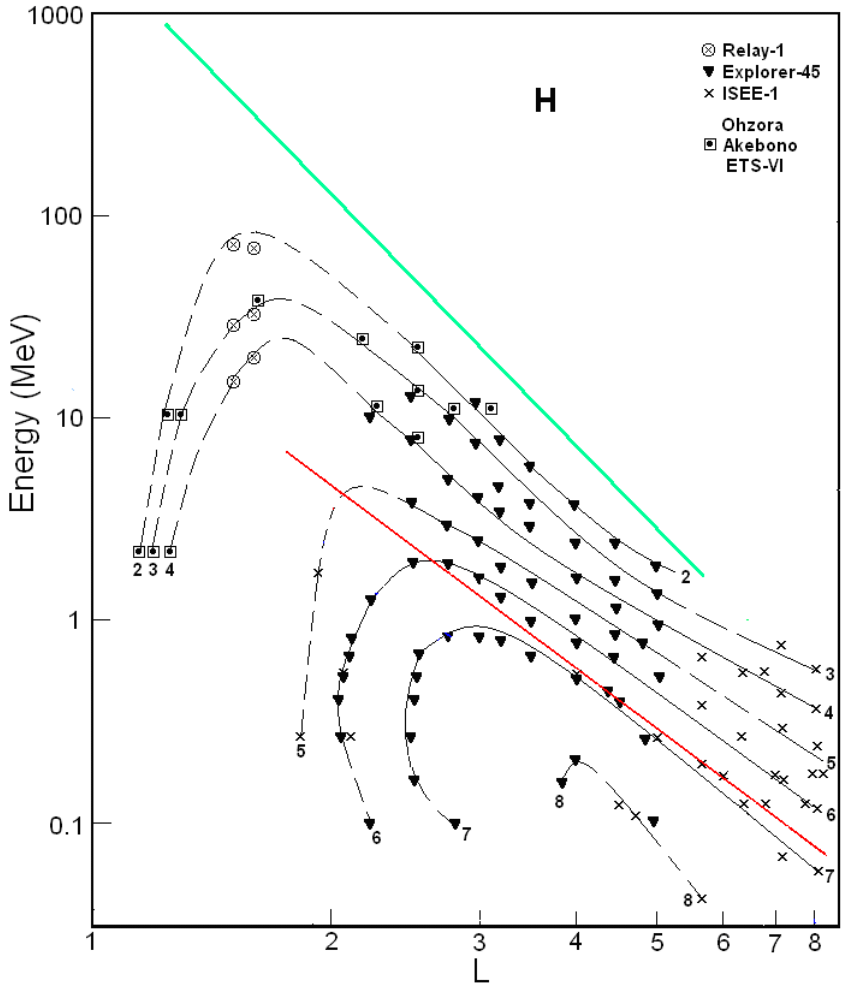

Figure 1. Proton fluxes in the ERB near minima of the solar activity. The numbers on the curves refer to the values of the decimal logarithms of J, which is given in units of $(\text{cm}^2\ \text{s ster MeV})^{-1}$, is the differential fluxes of protons with $\alpha_0 \approx 90^\circ$ (near the plane of the geomagnetic equator). Data of satellites are associated with different symbols. The red line corresponds to the lower boundary of the power-law tail of the proton spectra; while green line corresponds to the maximum energy of protons trapped in the ERB (Ilyin et al., 1984).

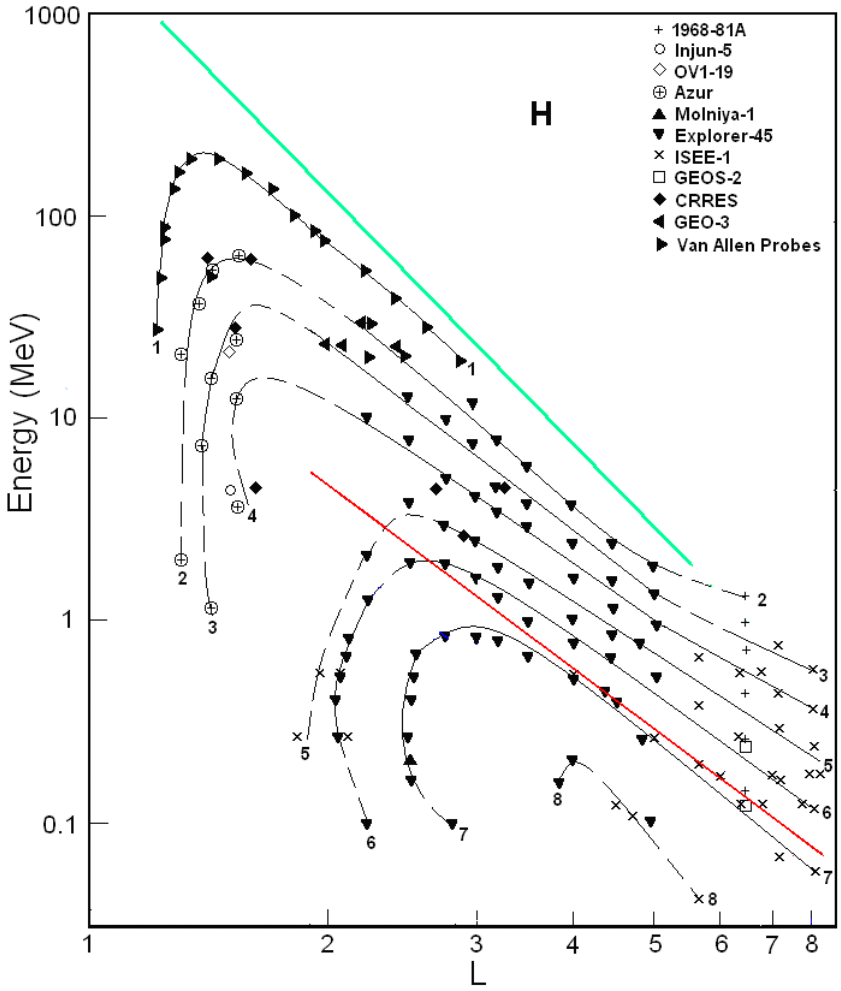

Figure 2. Proton fluxes in the ERB near maxima of the solar activity. The numbers on the curves refer to the values of the decimal logarithms of J, which is given in units of $(\text{cm}^2\ \text{s ster MeV})^{-1}$, is the differential fluxes of protons with $\alpha_0 \approx 90^o$ (near the plane of the geomagnetic equator). Data of satellites are associated with different symbols. The red line corresponds to the lower boundary of the power-law tail of the proton spectra; while green line corresponds to the maximum energy of protons trapped in the ERB (Ilyin et al., 1984).

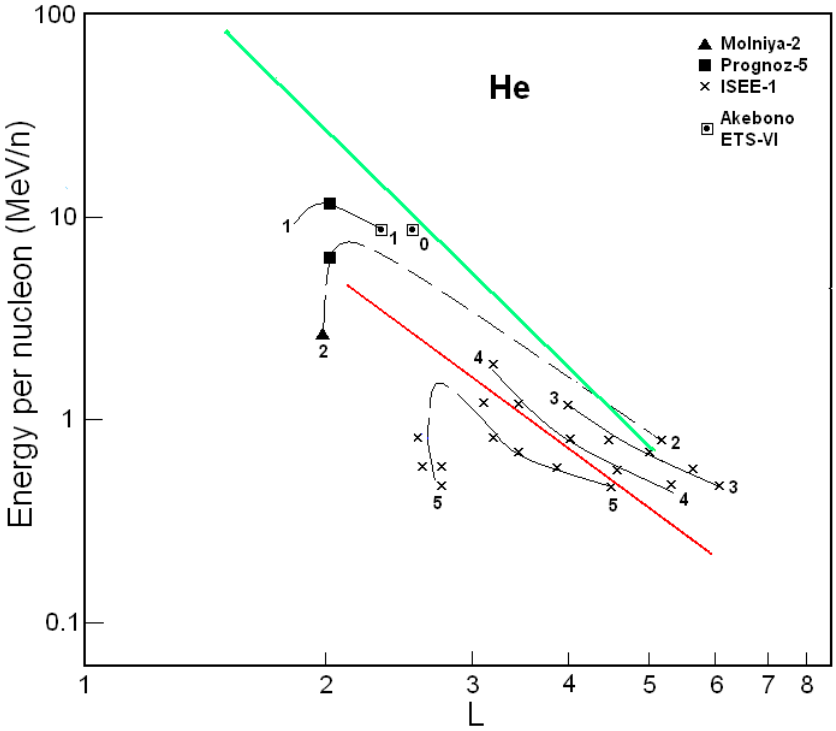

Figure 3. Helium ion fluxes in the ERB near minima of the solar activity. The numbers on the curves refer to the values of the decimal logarithms of J, which is given in units of $(\text{cm}^2\ \text{s ster MeV/n})^{-1}$, is the differential fluxes of helium ions with $\alpha_0 \approx 90^\circ$ (near the plane of the geomagnetic equator). Data of satellites are associated with different symbols. The red line corresponds to the lower boundary of the power-law tail of the helium spectra; while green line corresponds to the maximum energy of these ions trapped in the ERB (Ilyin et al., 1984).

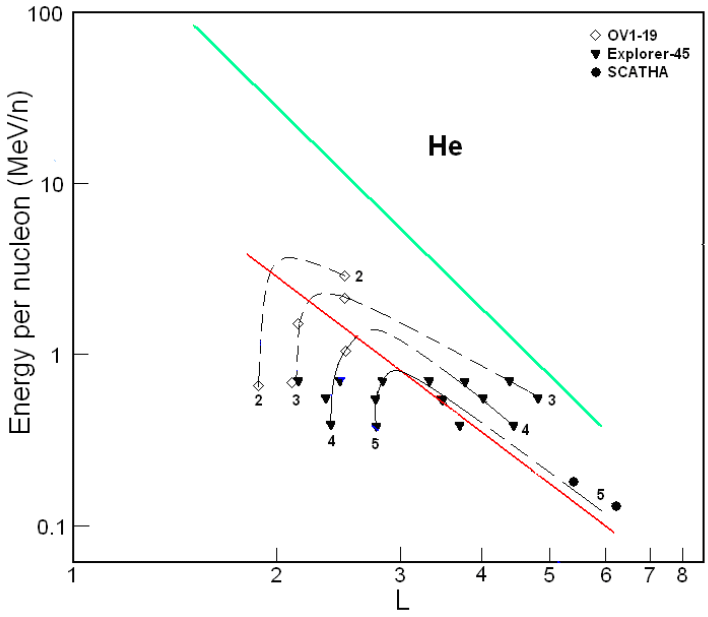

Figure 4. Helium ion fluxes in the ERB near maxima of the solar activity. The numbers on the curves refer to the value of the decimal logarithms of J which is given in units of $(\text{cm}^2\ \text{s ster MeV/n})^{-1}$, is the differential fluxes of ions with $\alpha_0 \approx 90^\circ$ (near the plane of the geomagnetic equator). Data of satellites are associated with different symbols. The red line corresponds to the lower boundary of the power-law tail of the helium spectra; while green line corresponds to the maximum energy of these ions trapped in the ERB (Ilyin et al., 1984).

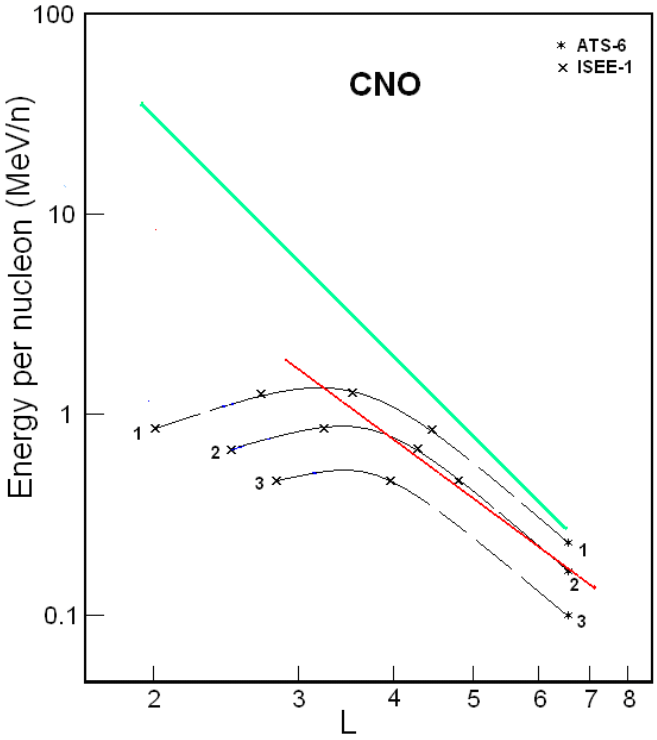

Figure 5. CNO ion fluxes in the ERB near minima of the solar activity. The numbers on the curves refer to the values of the decimal logarithms of J, which is given in units of $(\text{cm}^2\ \text{s ster MeV/n})^{-1}$, is the differential fluxes of ions with $\alpha_0 \approx 90^\circ$ (near the plane of the geomagnetic equator). Data of satellites are associated with different symbols. The red line corresponds to the lower boundary of the power-law tail of the CNO ion spectra; while green line corresponds to the maximum energy of these ions trapped in the ERB (Ilyin et al., 1984).

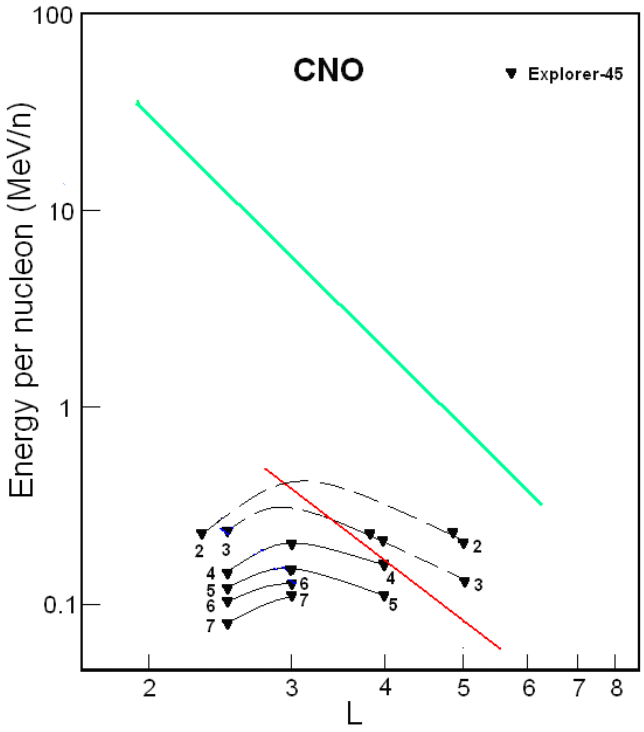

Figure 6. CNO ion fluxes in the ERB near the maximum of the solar activity. The numbers on the curves refer to the values of the decimal logarithms of J, which is given in units of $(\text{cm}^2\ \text{s ster MeV/n})^{-1}$, is the differential fluxes of ions with $\alpha_0 \approx 90^\circ$ (near the plane of the geomagnetic equator). Data of satellites are associated with different symbols. The red line corresponds to the lower boundary of the power-law tail of the CNO ion spectra; while green line corresponds to the maximum energy of these ions trapped in the ERB (Ilyin et al., 1984).